Water column methanotrophy controlled by a rapid oceanographic switch

Lea Steinle[1,2,*], Carolyn A. Graves[3], Tina Treude[2,4], Bénédicte Ferré[5], Arne Biastoch[2], Ingeborg Bussmann[6], Christian Berndt[2], Sebastian Krastel[7], Rachael H. James[3], Erik Behrens[2,8], Claus W. Böning[2], Jens Greinert[2,4,9], Célia-Julia Sapart[10,11], Markus Scheinert[2], Stefan Sommer[2], Moritz F. Lehmann[1] and Helge Niemann[1,*]

*Correspondence to: lea.steinle@unibas.ch, helge.niemann@unibas.ch

[1] Department of Environmental Sciences, University of Basel, 4056 Basel, Switzerland

[2] GEOMAR, Helmholtz Centre for Ocean Research Kiel, 24148 Kiel, Germany

[3] Ocean and Earth Science, National Oceanography Centre Southampton, Southampton SO14 3ZH, U.K.

[4] Present address: University of California, Los Angeles, Department of Earth, Planetary & Space Sciences and Atmospheric & Oceanic Sciences, Los Angeles CA 90095, USA

[5] CAGE-Centre for Arctic Gas Hydrate, Environment and Climate, Department of Geology, University of Tromsø, 9037 Tromsø, Norway

[6] Alfred Wegener Institute, Marine Station Helgoland, 27498 Helgoland, Germany

[7] Institute of Geosciences, University of Kiel, 24118 Kiel, Germany

[8] National Institute of Water and Atmospheric Research, Wellington 6021, New Zealand

[9] Royal Netherlands Institute for Sea Research NIOZ, Texel, The Netherlands

[10] Laboratoire de Glaciologie, Université Libre de Bruxelles, 1050 Brussels, Belgium

[11] Institute for Marine and Atmospheric Research, Utrecht University, 3584CC Utrecht, The Netherlands

Large amounts of the greenhouse gas methane are released from the seabed to the water column[1] where it may be consumed by aerobic methanotrophic bacteria[2]. This microbial filter is consequently the last marine sink for methane before its liberation to the atmosphere. The size and activity of methanotrophic communities, which determine the capacity of the water column methane filter, are thought to be mainly controlled by nutrient and redox dynamics[3-7], but little is known about the effects of ocean currents. Here we show that cold bottom water at methane seeps west off Svalbard, containing a large number of aerobic methanotrophs, was rapidly displaced by warmer water with a considerably smaller methanotrophic community. This water mass exchange, caused by short-term variations of the West Spitsbergen Current, constitutes an oceanographic switch severely reducing methanotrophic activity in the water column. Strong and fluctuating currents are widespread oceanographic features common at many methane seep systems and are thus likely to globally affect methane oxidation in the ocean water column.

Large amounts of methane are stored in the subsurface of continental margins as solid gas hydrates, gaseous reservoirs or dissolved in pore water[8]. At cold seeps, various physical, chemical, and geological processes force subsurface methane to ascend along pathways of structural weakness to the sea floor where a portion of this methane is utilised by anaerobic and aerobic methanotrophic microbes[1,9]. On a global scale, about 0.02 Gt yr^{-1} (3-3.5% of the atmospheric budget[10]) of methane bypasses the benthic filter system and is liberated to the ocean water column[1] where some of it is oxidised aerobically (aerobic oxidation of methane - MOx) (ref 2), or less commonly where the water column is anoxic, anaerobically (anaerobic oxidation of methane – AOM) (refs 2, 11). MOx is performed by methanotrophic bacteria (MOB) typically belonging to the Gamma- (type I) or Alphaproteobacteria (type II) (refs 12, 13):

$CH_4 + 2\ O_2 \rightarrow CO_2 + 2\ H_2O$

Water column MOx is consequently the final sink for methane before its release to the atmosphere, where it acts as a potent greenhouse gas. The water column MOx filter could become more

important in the future because environmental change may induce bottom water warming, which in turn may accelerate release of methane from the seafloor[14], in particular along the Arctic continental margins[15]. Despite the paramount importance of MOx for mitigating the release of methane to the atmosphere, little is known about environmental controls on the efficiency of the water column filter system. Known important factors determining the structure, activity and size of MOx communities are the availability of methane[5-7] and oxygen[3], or the abundance of trace metals (e.g. iron and copper) (refs 4, 7). Moreover, evolutionary adaptations to specific environmental conditions select for certain types of methanotrophs[13]. In addition to environmental selection, the physical transport of water masses harbouring distinct microbial communities has been identified as an important factor in shaping the biogeography of prokaryotic communities[16]. However, the potential effects of advective processes on the distribution of methanotrophs and the efficiency of the water column MOx filter system remain unconstrained[11,17,18].

During two research cruises to the Svalbard continental margin with R/V Poseidon (cruise POS419) and R/V Maria S. Merian (cruise MSM21/4) in August 2011 and 2012, respectively, we investigated methane dynamics and the activity levels and size of the water column MOx community in relation to water mass properties (Fig. 1). The Svalbard margin hosts an extensive, elongated (~22 km) cold seep system that is influenced by gas hydrates (Fig. 1a) (ref 19). Numerous gas flares emanate from the sea floor between the 350 and 400 m isobath[19,20], which corresponds to the landward termination of the gas hydrate stability zone. Seep sites have also been mapped on the shelf[19-21], and elevated methane levels have been observed in several of the fjords in the Svalbard archipelago[6,22,23].

The hydrodynamics west of Svalbard are governed by the West Spitsbergen Current (WSC), a 100 km-wide branch of the Norwegian Atlantic Current, which transports large amounts (up to 10 Sv) of warm and salty Atlantic Water (AW; >1°C, >35 psu) northward into the Fram Strait[24]. The WSC flows above cold Arctic Intermediate Water (AIW; <1°C, ~34.9 psu) (ref 25). It is steered topographically, and its eastern extension is constrained by the shelf break[26]. East of the WSC on

the shelf, the comparably slow East Spitsbergen Current transports cold and relatively fresh Arctic Water (ArW; <3°C, <34.8 psu) to the north[27].

During two sampling surveys in late August 2012, we measured methane concentrations, MOx activity and MOx biomass, as well as temperature, salinity and oxygen along a transect perpendicular to the line of the methane flares. The two mid-transect stations were at the MASOX site (named after the MASOX observatory[19]), which is located at 380 m water depth in the centre of the gas flare area both along slope and down slope. During both surveys, methane concentrations were highest in bottom waters, frequently exceeding 100 nmol L^{-1} (Fig. 1b). Surface water methane concentrations (9 nmol CH_4 L^{-1} on average) were ~3-fold supersaturated with respect to the local atmospheric equilibrium, indicating methane efflux to the atmosphere from this seep system[19]. Methane dissolved in the water column apparently originates from gas bubbles, which we observed visually during dives with the submersible *Jago*, and which were detected as flares in the middle of the transect with hydroacoustic single-beam systems[19]. Despite the constant supply of methane from the sea floor, we found considerable spatial and temporal variability in MOx activity (Fig. 1c, Supplementary Fig. 1). MOx was highest in bottom waters (>300 m water depth) during the first survey (Aug. 18/19) with methane turnover rates of up to 3.2 nmol L^{-1} d^{-1} (Fig. 1c, Tab. 1). These rates were similar to maximum rates detected at seeps on the Svalbard shelf[21] and in a nearby fjord[6]. In contrast, overall MOx activity was strongly reduced during the second survey (Aug. 30/31, Fig. 1c, Tab. 1). Consistent with the MOx activity measurements, cell enumeration conducted in the mid-transect region revealed a maximum in type I MOB cells on August 18/19 (up to 3.0×10^4 cells mL^{-1}; Tab. 1, Supplementary Fig. 1), but ~75% lower cell numbers during the second survey (up to 7.6×10^3 type I MOx cells mL^{-1}). The distributions of MOx activity and cell numbers translate to relatively constant, although low[12,28], cell-specific MOx rates of 1.54 to 1.66×10^{-2} fmol h^{-1} during the two sampling campaigns (Tab. 1). This constancy suggests that the efficiency of the methanotrophic filter system in the water column was controlled by the size of the MOx community

rather than by an environmental stimulus or suppression mechanism of MOx activity at the organismic level (Supplementary Fig. 2a, b).

Together with the reduction in MOx activity and community size, we observed a strong spatiotemporal change in the distribution of water mass properties. During the August 18/19 survey, bottom waters consisted of cold AW with admixture of AIW and ArW (Fig. 1d, e), which we subsequently refer to as cold AW (cAW). The cAW has water mass properties (temperature and salinity) akin to those of bottom waters found on the shelf[21]. By August 30/31, the cAW at the bottom was replaced by warmer Atlantic water (wAW, Fig. 1d, e). As the standing stock of methanotrophs in wAW was much lower compared to the cAW, rapid water mass exchange constitutes an oceanographic switch, causing a system-wide reduction of the efficiency of water column MOx. This apparent mechanistic link between MOx activity and the presence of either cAW or wAW is reflected in all water column profiles measured in 2012, as well as 2011 (Supplementary Figs. 1n, 2c).

We simulated the observed hydrodynamics using the high-resolution (1/20°, ~2.5 km grid space) VIKING20 model, which is nested in the global ocean/sea-ice model ORCA025 and represents ocean circulation variability in the northern North Atlantic at great verisimilitude[29] (Supplementary Fig. 3). For the WSC, the model yields two modes (offshore and nearshore) with respect to the meandering of the main, warm core of the WSC (Fig. 2, Supplementary Fig. 3d, e). During the offshore mode, the WSC separates into a warm offshore component and a cold undercurrent, which flows closely along the shelf break. The increase of the undercurrent causes stronger tilts of the isotherms and results in comparably cold bottom water temperatures. As a consequence, bottom waters at the shelf break and on the shelf are of similar density. The ArW on the shelf and fjord waters, both of which are characterised by a high MOx capacity[6,21], can thus be entrained downslope and contribute to the cAW, a situation that we observed during the August 18/19 survey. As a result, it is plausible that the high standing stock of methanotrophs in cAW partly originates from the shelf. The slow-flowing East Spitsbergen Current and the sheltered fjords lead to

comparably long water mass residence times, ensuring continuity of methane supply and supporting MOx community development in the shelf waters. During the nearshore mode, which is representative of the situation that we encountered during the August 30/31 survey, the warm core of the WSC flows closely along the shelf break, replacing the cAW with wAW and separating shelf and deeper AIW. The open-ocean origin of the WSC[24] makes an exposure to elevated methane concentrations in the history of the wAW unlikely, and could therefore explain the low standing stock of methanotrophs in this water mass.

The dynamics and magnitudes of bottom water temperatures and current velocities simulated by our model correspond well to recorded long-term measurements at the shelf break of the Svalbard margin[19,24]. Modelled and observational data indicate a transition time of 5-10 days between the two described modes. The meandering of the WSC appears to be associated with far-field variations and internal variability of the WSC, but this causality is non-linear so that the exact timing of the observed switch between the off- and nearshore mode cannot be predicted. Yet, both our model results as well as measured data from previous work[19,24] indicate that the WSC predominantly flows along the shelf break, whereas the offshore mode, with cAW at the bottom and a high MOx capacity in the water column, occurs only 15 % of the time.

At the Svalbard margin, methane flares were observed along a 22 km-long stretch of the upper slope at around 390 m water depth[19,20]. Our model results, together with the measurements of MOx activity and water mass properties, indicate that the entire area is similarly affected by water mass exchange. When spatially extrapolating MOx rate measurements from the transect samplings to the whole seep area (66 km^2), total MOx amounted to 0.28 t CH_4 d^{-1} on August 18/19, and was reduced by 66 % on August 30/31 (Tab. 1). Based on the maximum measurements, the capacity of the MOx filter in the studied seep area could well exceed 100 t CH_4 yr^{-1}, but this potential remains largely unexploited because the predominant nearshore mode of the WSC reduces MOx capacity to 45 t CH_4 yr^{-1}.

Similar to our measurements, varying MOx activities were detected in systems affected by differential circulation patterns and water mass mixing (Black Sea[11]; Santa Monica Basin[18]), and only low water column MOx activities were found at highly active methane seeps influenced by strong bottom currents (Hydrate Ridge[17]; Haakon Mosby Mud Volcano[30]). Currents result in relatively short water mass residence times above methane point sources, so that not enough time and continuity is provided for the development of large methanotrophic communities. Similarly, a well-established MOx community will be swept away from the methane source with the onset of water mass exchange. Dissolved methane, together with the methanotrophic community, will be dispersed leeward where ongoing MOx activity reduces methane concentrations further[7], most probably at rates controlled by the size of the MOx community. With respect to methane emission to the atmosphere, the impact of currents on water column MOx thus seems strongest in shallow-water cold seep environments, where the spatiotemporal distance between seafloor methane venting, water column methane consumption and methane evasion to the atmosphere is short. Most methane seeps are located along continental margins, where bottom water currents are commonly strong and fluctuating, as shown by our results from a global, high-resolution circulation model (ORCA12; Fig. 3, Supplementary Fig. 4). We thus argue that the variability of physical water mass transport is a globally important control on the distribution and abundance of methanotrophs and, as a consequence, on the efficiency of methane oxidation above point sources.

Data Availability:

All data presented in this paper are available in the PANGAEA data library (www.pangaea.de). In-depth information on the ORCA12 and VIKING20 models (data and code) will be provided on request.

References:

1. Boetius, A. & Wenzhofer, F. Seafloor oxygen consumption fuelled by methane from cold seeps. *Nat. Geosci.* **6,** 725-734 (2013).
2. Reeburgh, W. S. Oceanic methane biogeochemistry. *Chem. Rev.* **107,** 486-513 (2007).
3. Sansone, F. J. & Martens, C. S. Methane oxidation in Cape Lookout Bight, North Carolin. *Limnol. and Oceanogr.* **23,** 349-355 (1978).
4. Semrau, J. D., DiSpirito, A. A. & Yoon, S. Methanotrophs and copper. *FEMS Microbiol. Rev.* **34,** 496-531 (2010).
5. Kessler, J. D., Valentine, D. L., Redmond, M. C., Du, M. R., *et al.* A Persistent Oxygen Anomaly Reveals the Fate of Spilled Methane in the Deep Gulf of Mexico. *Science* **331,** 312-315 (2011).
6. Mau, S., Blees, J., Helmke, E., Niemann, H. & Damm, E. Vertical distribution of methane oxidation and methanotrophic response to elevated methane concentrations in stratified waters of the Arctic fjord Storfjorden (Svalbard, Norway). *Biogeosciences* **10,** 6267-6278 (2013).
7. Crespo-Medina, M., Meile, C. D., Hunter, K. S., Diercks, A. -R., *et al.* The rise and fall of methanotrophy following a deepwater oil-well blowout. *Nat. Geosci.* **7,** 423-427 (2014).
8. Wallmann, K., Pinero, E., Burwicz, E., Haeckel, M., *et al.* The Global Inventory of Methane Hydrate in Marine Sediments: A Theoretical Approach. *Energies* **5,** 2449-2498 (2012).
9. Knittel, K. & Boetius, A. Anaerobic Oxidation of Methane: Progress with an Unknown Process. *Annu. Rev. of Microbiol.* **63,** 311-334 (2009).
10. Kirschke, S., Bousquet, P., Ciais, P., Saunois, M., *et al.* Three decades of global methane sources and sinks. *Nat. Geosci.* **6,** 813-823 (2013).
11. Reeburgh, W. S., Ward, B. B., Whalen, S. C., Sandbeck, K. A., *et al.* Black-Sea Methane Geochemistry. *Deep-Sea Res. Pt. I* **38,** 1189-1210 (1991).
12. Hanson, R. S. & Hanson, T. E. Methanotrophic bacteria. *Microbiol. Rev.* **60,** 439-471 (1996).

13. Murrell, J. C. in *Handbook of Hydrocarbon and Lipid Microbiology* (eds Timmis, K. N.) 1953-1966 (Springer, Berlin, 2010).
14. Ferré, B., Mienert, J. & Feseker, T. Ocean temperature variability for the past 60 years on the Norwegian-Svalbard margin influences gas hydrate stability on human time scales. *J. Geophy. Res.-Oceans* **117,** 10.1029/2012JC008300 (2012).
15. Biastoch, A., Treude, T., Rüpke, L. H., Riebesell, U., *et al.* Rising Arctic Ocean temperatures cause gas hydrate destabilization and ocean acidification. *Geophys. Res. Lett.* **38,** DOI: 10.1029/2011GL047222 (2011).
16. Wilkins, D., van Sebille, E., Rintoul, S. R., Lauro, F. M. & Cavicchioli, R. Advection shapes Southern Ocean microbial assemblages independent of distance and environment effects. *Nat. Commun.* **4,** (2013).
17. Heeschen, K. U., Collier, R. W., de Angelis, M. A., Suess, E., *et al.* Methane sources, distributions, and fluxes from cold vent sites at Hydrate Ridge, Cascadia Margin. *Glob. Biogeochem. Cy.* **19,** (2005).
18. Heintz, M. B., Mau, S. & Valentine, D. L. Physical control on methanotrophic potential in waters of the Santa Monica Basin, Southern California. *Limnol. Oceanogr.* **57,** 420-432 (2012).
19. Berndt, C., Feseker, T., Treude, T., Krastel, S., *et al.* Temporal Constraints on Hydrate-Controlled Methane Seepage off Svalbard. *Science* **343,** 284-287 (2014).
20. Westbrook, G. K., Thatcher, K. E., Rohling, E. J., Piotrowski, A. M., *et al.* Escape of methane gas from the seabed along the West Spitsbergen continental margin. *Geophys. Res. Lett.* **36,** (2009).
21. Gentz, T., Damm, E., Schneider von Deimling, J., Mau, S., *et al.* A water column study of methane around gas flares located at the West Spitsbergen continental margin. *Cont. Shelf Res.* **72,** 107-118 (2014).

22. Damm, E., Mackensen, A., Budéus, G., Faber, E. & Hanfland, C. Pathways of methane in seawater: Plume spreading in an Arctic shelf environment (SW-Spitsbergen). *Cont. Shelf Res.* **25,** 1453-1472 (2005).

23. Damm, E., Kiene, R. P., Schwarz, J., Falck, E. & Dieckmann, G. Methane cycling in Arctic shelf water and its relationship with phytoplankton biomass and DMSP. *Mar. Chem.* **109,** 45-59 (2008).

24. Schauer, U., Fahrbach, E., Osterhus, S. & Rohardt, G. Arctic warming through the Fram Strait: Oceanic heat transport from 3 years of measurements. *J. Geophy. Res.-Oceans* **109,** 14 (2004).

25. Blindheim, J. Arctic intermediate water in the Norwegian sea. *Deep-Sea Res. Pt. I* **37,** 1475-1489 (1990).

26. Bourke, R. H., Weigel, A. M. & Paquette, R. G. The westward turning branch of the West Spitsbergen Current. *J. Geophy. Res.-Oceans* **93,** 14065-14077 (1988).

27. Loeng, H. Features of the physical oceanographic conditions of the Barents Sea. *Polar Res.* **10,** 5-18 (1991).

28. Carini, S., Bano, N., LeCleir, G. & Joye, S. B. Aerobic methane oxidation and methanotroph community composition during seasonal stratification in Mono Lake, California (USA). *Environ. Microbiol.* **7,** 1127-1138 (2005).

29. Fischer, J., Karstensen, J., Zantopp, R., Visbeck, M., *et al.* Intra-seasonal variability of the DWBC in the western subpolar North Atlantic. *Prog. Oceanogr.* 10.1016/j.pocean.2014.04.002 (2014).

30. Sauter, E. J., Muyakshin, S. I., Charlou, J. L., Schluter, M., *et al.* Methane discharge from a deep-sea submarine mud volcano into the upper water column by gas hydrate-coated methane bubbles. *Earth Planet. Sc. Lett.* **243,** 354-365 (2006).

Correspondence and requests for materials should be addressed to helge.niemann@unibas.ch and lea.steinle@unibas.ch.

Acknowledgements

We thank the Captains, crews and shipboard scientific parties of R/V Poseidon and R/V Maria S. Merian for their help at sea. This work received financial support through a D-A-CH project funded by the Swiss National Science Foundation and German Research foundation (grant no. 200021L_138057). Further support was provided through the EU COST Action PERGAMON (ESSEM 0902), a Postgraduate Scholarship of the National Research Council of Canada, the Centre of Excellence "CAGE" funded by the Norwegian Research Council (grant no. 223259) and the Cluster of Excellence "The Future Ocean" funded by the German Research Foundation.

Supplementary materials, including the methods, are available on line at www.nature.com/XXXX.

Author Contributions

L.S., C.G., T.T., I.B., J.G., C.J.S. S.S. and H.N. collected the samples and performed measurements of biogeochemical rates and/or physicochemical parameters. L.S. carried out enumeration of microbial cells. A.B., B.F., J.G., E.B., C.W.B. and M.S. conducted oceanographic modelling, interpretation and/or graphical representation. C.B. and S.K. were responsible for acoustic measurements. H.N., T.T., R.H.J. and M.F.L supervised research. L.S. and H.N led the development of the manuscript and all co-authors contributed to data interpretation and writing of manuscript.

The authors declare no competing financial interests.

Figure/Table Captions:

Fig.1: Study area and distribution of aerobic methanotrophy and physicochemical parameters above methane seeps at the Svalbard continental margin. **a,** Map of the seep system with numerous methane flares (grey stars) emanating from the sea floor around the depth of the landward termination of the gas hydrate stability zone. Sampling locations are indicated (squares: POS419, 2011; circles: MSM21/4, 2012). Distribution of **b,** methane, **c,** aerobic methane oxidation rates (r_{MOx}), **d,** temperature and **e,** salinity measured during two sampling surveys along the same transect crossing the MASOX site[19]. **b-e**, Positions of discrete samples (crosses) and continuous measurements (lines) are indicated.

Fig. 2: Modelled cross-slope distribution of water column temperature and current velocity in the West Spitsbergen Current. Modelled time-averaged water column temperature (°C), sigma-t (green contours, kg m^{-3}-1000) and current velocity (black contours, cm s^{-1}) for **a,** cold temperature anomalies, **b,** mean temperature and **c,** warm temperature anomalies. Anomalies were defined as one standard deviation below or above the seasonally and interannually varying temperature mean in bottom waters at the MASOX site (cross mark; cf. Supplementary Fig. 3c). During times of cold temperature anomalies, the WSC is in its offshore mode, with a cold undercurrent along the slope.

Fig. 3: Modelled bottom current velocity at methane seeps. Modelled (1/12° resolution) mean annual (year 2000) bottom water current velocities for bottom depths between 100 and 2500 m. Current velocities at continental margins, where most methane seeps are located, frequently exceed

10 cm s^{-1} and can be highly variable (cf. Supplementary Fig. 4). Locations of selected methane seeps are indicated by white circles.

Tab. 1: Comparison of methane consumption and methanotrophic cell numbers between the two transect sampling campaigns in 2012. Total CH_4 oxidised in the seep area was calculated by extrapolation of average MOx rates calculated for each sampling date to the total seep-affected water mass volume (3 km width × 22 km length × 0.388 km average water depth). Highest MOB cell numbers and fraction (in %) of total cell numbers are indicated. Cell-specific MOx rates represent the average of all samples counted on the respective transects (±standard error. n=12, Aug. 18/19; n=15, Aug. 30/31).

Supplementary Information

Water column methanotrophy controlled by a rapid oceanographic switch

Lea Steinle[1,2,*], Carolyn A. Graves[3], Tina Treude[24], Bénédicte Ferré[5], Arne Biastoch[2], Ingeborg Bussmann[6], Christian Berndt[2], Sebastian Krastel[7], Rachael H. James[3], Erik Behrens[2,8], Claus W. Böning[2], Jens Greinert[2,4,9], Markus Scheinert[2], Célia-Julia Sapart[10,11], Stefan Sommer[2], Moritz F. Lehmann[1] and Helge Niemann[1,*]

*Correspondence to: lea.steinle@unibas.ch, helge.niemann@unibas.ch

[1] Department of Environmental Sciences, University of Basel, 4056 Basel, Switzerland

[2] GEOMAR, Helmholtz Centre for Ocean Research Kiel, 24148 Kiel, Germany

[3] Ocean and Earth Science, National Oceanography Centre Southampton, Southampton SO14 3ZH, U.K.

[4] Present address: University of California, Los Angeles, Department of Earth, Planetary & Space Sciences and Atmospheric & Oceanic Sciences, Los Angeles CA 90095, USA

[5] CAGE-Centre for Arctic Gas Hydrate, Environment and Climate, Department of Geology, University of Tromsø, 9037 Tromsø, Norway

[6] Alfred Wegener Institute, Marine Station Helgoland, 27498 Helgoland, Germany

[7] Institute of Geosciences, University of Kiel, 24118 Kiel, Germany

[8] National Institute of Water and Atmospheric Research, Wellington 6021, New Zealand

[9] Royal Netherlands Institute for Sea Research NIOZ, Texel, The Netherlands

[10] Laboratoire de Glaciologie, Université Libre de Bruxelles, 1050 Brussels, Belgium

[11] Institute for Marine and Atmospheric Research, Utrecht University, 3584CC Utrecht, The Netherlands

1. Physiochemical and biogeochemical water column parameters

1.1 Temperature and salinity

Temperature and salinity were measured with a Seabird SBE911 CTD (CTD: conductivity/temperature/density probe; Seabird-Electronics, USA) equipped with dual temperature and conductivity sensors. For monitoring sensor performance, we conducted several CTD casts with a third set of temperature and conductivity sensors (SAIV A/S SN363, Norway, calibrated by SAIV A/S directly before the cruise). The offsets between the Seabird and SAIV were ≤0.01°C and ≤0.04 psu. During the MSM21/4 cruise, most CTD casts were taken at the MASOX site (78°33.3'N, 9°28.6'E; ~380 m water depth; ref 1) and/or along a transect crossing this site. One additional CTD cast was performed ~6.4 km further north at the HyBIS site (78°36.68'N, 009°25.50'E; cf. Fig. 1a; ref 1). During the POS419 cruise, CTD casts were also performed using a Seabird SBE911 device at three stations between the MASOX and HyBIS site and at one station ~8.8 km south of the MASOX site (Fig. 1a). For a complete station list see Supplementary Tab. 1.

1.2 Methane concentrations

For analysis of methane concentrations and MOx rates at discrete water depths, we sampled the water column with 24 × 10 L PTFE-lined Niskin bottles mounted on a CTD/Rosette sampler and sub-samples were taken immediately upon recovery of the sampler[1]. During the MSM21/4 cruise, methane was analysed with a headspace technique and gas chromatography with flame ionisation detection[1]. Briefly, ~ 600 mL seawater was subsampled bubble-free into triple-layer Evarex Barrier Bags (Oxford Nutrition, U.K.) followed by the addition of a headspace (20 mL N_2) and equilibration for several hours. Methane concentrations were determined by gas chromatography (Agilent 7890A GC; 80/100 mesh HayeSep Q packed stainless steel column, 1.83 m length, 2 mm i.d.; flame ionization detector set at 250 °C; oven operated isocratically at 60 °C; N_2 carrier gas at 33 mL min^{-1}) from a 2 mL aliquot of the headspace. The GC system was calibrated with external standards (20 ppm methane standard, Air Liquide, Germany), and reproducibility (determined by 3

replicate analyses of an individual sample) was < ± 5 %. During the POS419 cruise, methane concentrations were analysed with a slightly modified headspace method with respect to sampling vials (120 mL glass vials, 5 mL N_2 headspace, fixed with 0.5 mL saturated aqueous $HgCl_2$ solution) and manufacturers of analytical instruments (Thermo Scientific FOCUS GC, direct injection; Resteck packed column HayeSep Q 80/100, 2 m length, 2 mm i.d.; flame ionization detector set at 170 °C; oven temperature was ramped from 40 to 120 °C in steps, H_2 carrier gas at 33 mL min^{-1}). Seawater methane concentrations and the degree of saturation with respect to the atmospheric equilibrium were calculated with consideration of sample and headspace volume, temperature, salinity, atmospheric pressure and atmospheric CH_4 mixing ratio[2,3].

1.3 Methane oxidation rates

MOx rates were determined at sea from *ex situ* incubations with trace amounts of tritium-labelled methane (^3H-CH_4) similarly to published methods[4,5] with some modifications[6]. For each depth, four crimp-top vials (20 mL) were filled bubble-free and closed with bromobutyl stoppers (Helvoet Pharme, Belgium), amended with 10 µl gaseous ^3H-CH_4/N_2 mixture (~25 kBq, <50 pmol CH_4, American Radiolabeled Chemicals, USA) and incubated for 72 h at *in situ* temperature in the dark. Linearity of MOx during the incubation time period (~72 h) was confirmed by replicate incubations at 24, 48 and 72 h. MOx rates were corrected for (insubstantial) tracer turnover in killed controls (addition of 100 µl, saturated aqueous $HgCl_2$ solution). Rates on the POS419 cruise were measured analogously, but instead of 20 ml we incubated in 120 ml bromobutyl-sealed (Ochs, Germany) crimp top vials with an amendment of 100 µl tracer gas. Single or triplicate incubations were conducted for each depth. MOx rates were calculated from the fractional turnover of labelled CH_4 and water column CH_4 concentration assuming first order kinetics[5]. Average standard deviation between replicates was ±20.4 % for MSM21/4 incubations and ±38 % for POS419 incubations.

1.4 Biomass estimation of methanotrophs

The identity and abundance of aerobic methanotrophic bacteria (MOB) was investigated by catalysed reporter deposition fluorescence *in situ* hybridisation (CARD-FISH; refs 7,8) from samples collected during the MSM 21/4 cruise. A 100 ml seawater aliquot was fixed for ~4 h with formaldehyde (1.5 % final concentration) at 4 °C. The fixed sample was filtered through a polycarbonate filter (Whatman Nuclepore black track-etched polycarbonate membrane filter, 25 mm diameter, 0.2 µm pore size) with a gentle vacuum-pressure of 0.5 bar. Filters were air-dried and stored at -20 °C until further analyses. Cells embedded on the filter were permeabilised with lysozyme[7], followed by inactivation of endogenous peroxidases in a 0.15 % H_2O_2/methanol solution for 30 min at room temperature. Filters were then washed successively in sterile MilliQ (1 min) and aqueous ethanol solution (96 %, v/v; 2 min) and finally air-dried. Filters were hybridised with ~300 µl hybridisation buffer for 3 h at 46 °C. The buffer contained either a mix of probes Mγ705-HRP and Mγ84-HRP (0.3 ng μL^{-1} each), or probe Mα450-HRP (0.6 ng μL^{-1}) for the detection of Type I and Type II MOx communities, respectively[9]. Negative controls (sulphide-oxidizing mixed culture, enriched from a freshwater lake) were used to ensure specificity of probe binding with our hybridisation conditions. Catalysed reporter deposition and DAPI staining was carried out according to published recommendations[8] with an amplification time of 20 min at 37 °C in a buffer containing 1 µL of the labelled tyramide (Alexa488: Invitrogen A20000, lot 1252193; USA). Filters were finally washed for 10 min in PBS. We used Citifluor AF1 (Citifluor Ltd., U.K.) as mountant for fluorescence microscopy. CARD-FISH- and DAPI-stained samples were examined with an epifluorescence microscope (Leica DM2500 equipped with the external ultraviolet light source, EL6000) at a 1000-fold magnification. For each sample, ~1000 DAPI-stained cells in ≥ 10 microscopic fields were counted. Total cell numbers in the lowest 200 m of the water column were similar between sampling dates ($2.09 \pm 0.14 \times 10^5$ cells mL^{-1}), while surface water generally contained higher cell numbers (up to 10.8×10^5 cells mL^{-1}) with higher variations between sampling dates (data not shown).

Type I MOB cells occurred as single/double cells (Supplementary Fig. 1m) or as loose 'aggregates' (Supplementary Fig. 1j). To account for the heterogeneous distribution of the aggregates, we counted 70 microscopic fields for each sample (average StDev. of MOB cell numbers between grids for one sample: ± 37%). Type II MOB cells accounted for less than 1 % of all MOB cells (data not shown), and were thus of minor importance for the water column MOx filter capacity.

Water samples collected at the MASOX site during the MSM21/4 cruise concomitantly showed elevated type I MOB cell numbers and MOx rates (Supplementary Fig. 1). Vice versa, water samples characterised by low MOx rates generally contained low numbers of MOB cells. Although MOx was maximal in bottom waters with elevated methane concentrations (Fig. 1c, Supplementary Fig. 1), we frequently encountered low levels of MOx activity (and methanotrophic biomass) in bottom water samples with high methane concentrations. MOx activity was thus determined by MOx biomass rather than methane substrate availability (Supplementary Figs. 2a, b). Furthermore, together with the MOx community size, the MOx filter capacity (see MOx rates in Supplementary Fig. 1) was only elevated in relatively cold and saline bottom waters (<4 °C, >34.9 psu, Supplementary Fig. 2c), which were only present during the offshore mode of the West Spitsbergen Current (WSC).

1.5 Interpolation and extrapolation of physiochemical and biogeochemical water column parameters.

Values of physiochemical and biogeochemical water column parameters were measured at discrete stations, and, in case of methane concentration and MOx activity, in discrete water depths, during the transect sampling campaigns (Aug. 18/19 and 30/31). Depth-integrated areal MOx rates were determined by linear interpolation between measured rates and extrapolation to a water column of 1 m^2. For representation as contour plots (Fig 1b-e), discrete values were linearly interpolated by using the Matlab software package. For extrapolating MOx rates to the known seep area, we first calculated weighted averages from the interpolated MOx rates (Fig. 1c) for the two sampling

campaigns. These averages (0.7 and 0.2 nmol L^{-1} d^{-1} for Aug. 18/19 and 30/31, respectively) were then extrapolated to the whole water volume in the seep area (3 km width × 22 km length × 0.388 km average water depth).

2. Regional hydrographic changes in a wider oceanographic context

For a deeper understanding of the hydrographic changes west off the Svalbard shelf and the interplay with the large-scale circulation, we utilised 5-daily output from the VIKING20 model, a high-resolution ocean/sea-ice simulation[10,11]. Based on the NEMO code[12], VIKING20 has a 1/20° grid cell size of the subpolar/subarctic North Atlantic (32°N - 85°N) (ref 10) and is two-way nested[13] in a global 1/4° configuration (ORCA025 grid; ref 11). It is forced by atmospheric data covering synoptic (6-hourly to daily), seasonal, interannual to decadal timescales of the years 1948-2007 (ref 11). With a ~2.5 km grid space off West-Spitsbergen and 46 vertical levels (20 in the upper 500 m), VIKING20 realistically captures both the large-scale circulation and the mesoscale variability in the subpolar/subarctic North Atlantic by great verisimilitude[14], both with detailed mean flow characteristics[15] and temporal variability on short-term to decadal time scales[16]. The circulation in the Fram Strait, for instance, shows the same variability along the eastern boundary, with northward velocities up to 40 cm s^{-1} and beyond, as observed by Schauer et al., 2004 (ref 17). Modelled bottom current velocity (Fig. 2) agrees well with measurement data from the MASOX observatory (10 cm s^{-1} on average; ref 1).

Water column temperatures at the MASOX site (Supplementary Fig. 3a, b) greatly vary on seasonal and interannual timescales, but also show distinct minima and maxima (Supplementary Fig. 3c) strongly deviating from the (seasonally and interannually varying) temperature mean. These minima and maxima are caused by the variable position of the main, warm core of the WSC. Supplementary Fig. 3d shows time-averaged circulation patterns of the WSC along the offshore flank of the study area at 300 m water depth (the MASOX position is indicated with a cross mark). During time periods of cold bottom water temperature anomalies (i.e., greater than one standard

deviation below the seasonally and interannually varying temperature mean; blue line in Supplementary Fig. 3c), the main core of the WSC is located offshore, giving rise to a cold undercurrent at the shelf break (Supplementary Fig. 3d), and thus to the observed and modelled cold bottom water temperatures at the shelf break. The comparably strong northward tilting of the flares that we observed during hydroacoustic surveys just before our samplings on August 17 and 18/19 (data not shown) indicates the presence of this fast undercurrent. In contrast, when the main core is meandering to the shore, the warm water of the WSC replaces the cold bottom water, resulting in the rise of bottom water temperatures. This nearshore mode corresponds to observed and modelled average and anomalously warm bottom water temperatures (i.e., values above one standard deviation above the seasonally and interannually varying temperature mean; red line in Supplementary Fig. 3c). The time-averaged circulation pattern of the nearshore mode is shown in Supplementary Fig. 3e. The meandering of the main core is caused by far-field and internal variations of the WSC, leading to a nonlinear behavior of the current with transition times between offshore- and nearshore mode of 5-10 days.

Global bottom water velocities at continental margins were analyzed using a global variant of the ocean/sea-ice model at 1/12° resolution (ORCA12). Similar to VIKING20, this model has been forced by atmospheric data[14], but over a shorter timeframe (1978-2003). Highly variable near-bottom currents are common along continental slopes and below regions of strong surface currents[18].

Supplementary Figure Captions:

Supplementary Figure 1: Methane concentrations, methane oxidation rates and methanotrophic cell numbers from repeated sampling campaigns at the MASOX station. a-i, Methane concentration (red), methane oxidation rates (grey), and **b, c, d, g, h,** cell numbers of type I aerobic methanotrophic bacteria (MOB; green), at the MASOX site measured during the MSM21/4 cruise at different dates (chronological station numbers are indicated in blue). Error bars of MOx represent standard deviation (n=4). **j-m,** Micrographs of water column microbes from samples collected at 380 m water depth at the MASOX site (station 554). Type I MOB cells were quantified by CARD-FISH (**j, m**; in green; mixture of probes Mγ705-HRP and Mγ84-HRP) and DAPI (=total cells; **k, l,** in blue) staining, followed by epifluorescence microscopy. The scale bar represents 10 µm. Type I MOB cells occurred as **m,** single/double cells, or **j,** as loose 'aggregates'. Stations 554/555 and 637/638 were sampled during transect samplings on Aug. 18/19 and Aug. 30/31, respectively. **n,** Maximum and depth integrated MOx rates at the MASOX site (cf. **a-g**) in relation to the presence of cAW or wAW at the sea floor. Together with the MOx community size, the MOx filter capacity was only elevated in relatively cold and saline bottom waters (<4 °C, >34.9 psu; cf. Supplementary Fig. **2a**), which were solely present during the offshore mode of the WSC.

Supplementary Figure 2: Aerobic methane oxidation in relation to bottom water properties. **a,** Methane oxidation rates (r_{MOX}) in relation to **a,** cell numbers of type I aerobic methane oxidising bacteria, **b** methane concentration and, **c** salinity and temperature, measured during the MSM21/4 (cyan dots) and POS419 (pink squares) cruise. Note that MOB cell numbers were only determined from selected samples from the MASOX site collected during the MSM21/4 cruise, while methane concentration, salinity and temperature were determined for all samples designated

for MOx rate measurements. Linear correlation for **b**, includes all samples from MSM21/4 and POS419.

Supplementary Figure 3: Modelled temporal progression of water temperature and circulation patterns of the WSC. Temperature distribution in **a,** the entire water column (surface to bottom), and **b**, bottom waters (300 m water depth), as well as **c**, bottom water temperature corrected for seasonal and interannual temperature variations at the MASOX site. **d,** Time-averaged circulation patterns of the WSC at 300 m water depth during the offshore mode (temperature anomaly against long-term average, colour-coded, °C), and **e**, the nearshore mode (long-term averaged temperature, colour-coded, °C). The MASOX position is indicated with a cross mark. Current velocities are indicated as black arrows and wind forcing as green arrows. The vertical distribution of time-averaged temperature, density and current velocity, respectively, along a cross-section over the MASOX site (black line) is shown in Fig. 2.

Supplementary Figure 4: Modelled bottom current velocity and standard deviation of current velocities at methane seeps. a, Modelled (1/12° resolution) mean annual (year 2000) bottom water current velocities and, **b**, standard deviation of bottom current velocities (based on 5-day averages) for bottom depths between 100 and 2500 m. Bottom current velocities at continental margins, where most methane seeps are located, frequently exceed 10 cm s^{-1} and are highly variable. Standard deviations typically exceed 50% of the mean flow. Locations of selected methane seeps are indicated by white circles.

Supplementary Table 1: List of Stations sampled during the POS419 and MSM21/4 cruises. The numbers of bottles sampled per CTD cast are indicated.

Supplementary References

1. Berndt, C., Feseker, T., Treude, T., Krastel, S., *et al.* Temporal Constraints on Hydrate-Controlled Methane Seepage off Svalbard. *Science* **343,** 284-287 (2014).
2. Wiesenburg, D. A. & Guinasso, N. L. Equilibrium solubilities of methane, carbon monoxide, and hydrogen in water and sea water. *J. Chem. Eng. Data* **24,** 356-360 (1979).
3. Fisher, R. E., Sriskantharajah, S., Lowry, D., Lanoisellé, M., *et al.* Arctic methane sources: Isotopic evidence for atmospheric inputs. *Geophys. Res. Lett.* **38,** DOI: 10.1029/2011GL049319 (2011).
4. Valentine, D. L., Blanton, D. C., Reeburgh, W. S. & Kastner, M. Water column methane oxidation adjacent to an area of active hydrate dissociation, Eel River Basin. *Geochim. Cosmochim. Ac.* **65,** 2633-2640 (2001).
5. Reeburgh, W. S. Oceanic methane biogeochemistry. *Chem. Rev.* **107,** 486-513 (2007).
6. Niemann, H., Steinle, L., Blees, J. H., Krause, S., *et al.* Toxic effects of butyl elastomers on aerobic methane oxidation. *Limnolog and Oceanography: Methods.* **in press** (2015).
7. Pernthaler, A., Pernthaler, J. & Amann, R. Fluorescence In Situ Hybridization and Catalyzed Reporter Deposition for the Identification of Marine Bacteria. *Appl. Env. Microb.* **68,** 3094-3101 (2002).
8. Pernthaler, A. & Pernthaler, J. Fluorescence in situ hybridization for the identification of environmental microbes. *Methods Mol. Biol.* **353,** 153-164 (2007).
9. Eller, G., Stubner, S. & Frenzel, P. Group-specific 16S rRNA targeted probes for the detection of type I and type II methanotrophs by fluorescence in situ hybridisation. *FEMS Microbiol. Lett.* **198,** 91-97 (2001).
10. Behrens, E. *The oceanic response to Greenland melting: the effect of increasing model resolution* (Christian Albrechts University, Kiel , Germany, 2013).
11. Behrens, E., Biastoch, A. & Böning, C. W. Spurious AMOC trends in global ocean sea-ice models related to subarctic freshwater forcing. *Ocean Model.* **69,** 39-49 (2013).

12. Madec, G. *Nemo ocean engine, Note du Pole de modélisation, Institut Pierre-Simon Laplace (IPSL) No 27, France* 2008).

13. Debreu, L., Vouland, C. & Blayo AGRIF: Adaptive Grid Refinement in Fortran. *Comput. Geosci.* **34,** 8-13 (2008).

14. Large, W. G. & Yeager, S. G. The global climatology of an interannually varying air–sea flux data set. *Clim. Dynam.* **33,** 341-364 (2009).

15. Mertens, C., Rhein, M., Walter, M., Böning, C. W., *et al.* Circulation and transports in the Newfoundland Basin, western subpolar North Atlantic. *J. Geophys. Res.-Oceans* **119,** 7772-7793 (2014).

16. Fischer, J., Karstensen, J., Zantopp, R., Visbeck, M., *et al.* Intra-seasonal variability of the DWBC in the western subpolar North Atlantic. *Prog. Oceanogr.* 10.1016/j.pocean.2014.04.002 (2014).

17. Schauer, U., Fahrbach, E., Osterhus, S. & Rohardt, G. Arctic warming through the Fram Strait: Oceanic heat transport from 3 years of measurements. *J. Geophys. Res.-Oceans* **109,** 14 (2004).

18. Cronin, M. F., Tozuka, T., Biastoch, A., Durgadoo, J. V. & Beal, L. M. Prevalence of strong bottom currents in the greater Agulhas system. *Geophys. Res. Lett.* **40,** 1772-1776 (2013).

Fig. 1

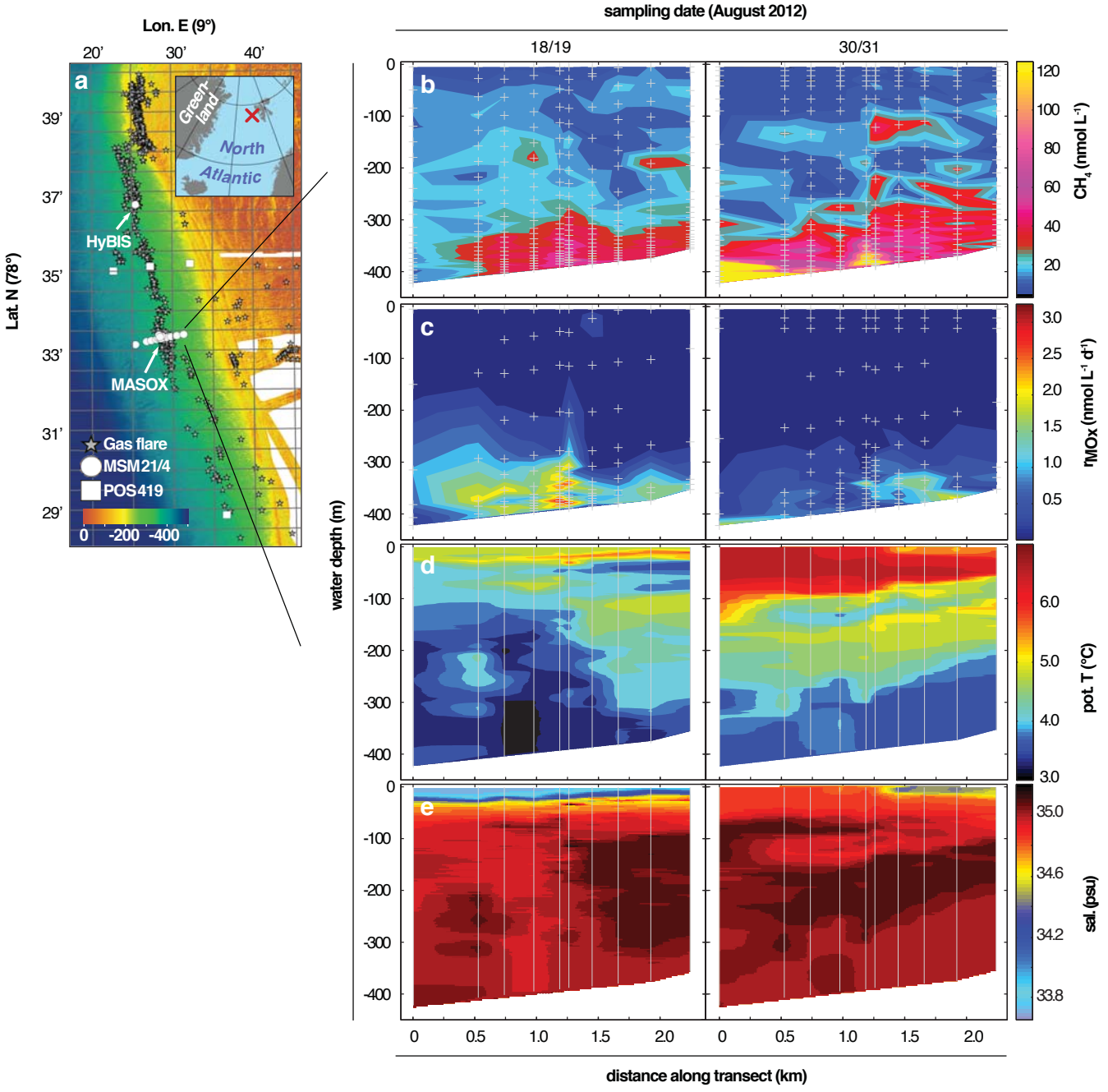
Lon. E (9°)
20'
30'
40'
Lat. N (78°)
39'
37'
35'
33'
31'
29'
a
Green land
North Atlantic
HyBIS
MASOX
Gas flare
MSM21/4
POS419
0
-200
-400
sampling date (August 2012)
18/19
30/31
b
c
d
e
water depth (m)
0
-100
-200
-300
-400
0
0.5
1.0
1.5
2.0
distance along transect (km)
CH4 (nmol L-1)
120
100
80
60
40
20
rMOx (nmol L-1 d-1)
3.0
2.5
2.0
1.5
1.0
0.5
pot. T (°C)
6.0
5.0
4.0
3.0
sal. (psu)
35.0
34.6
34.2
33.8

Fig. 2

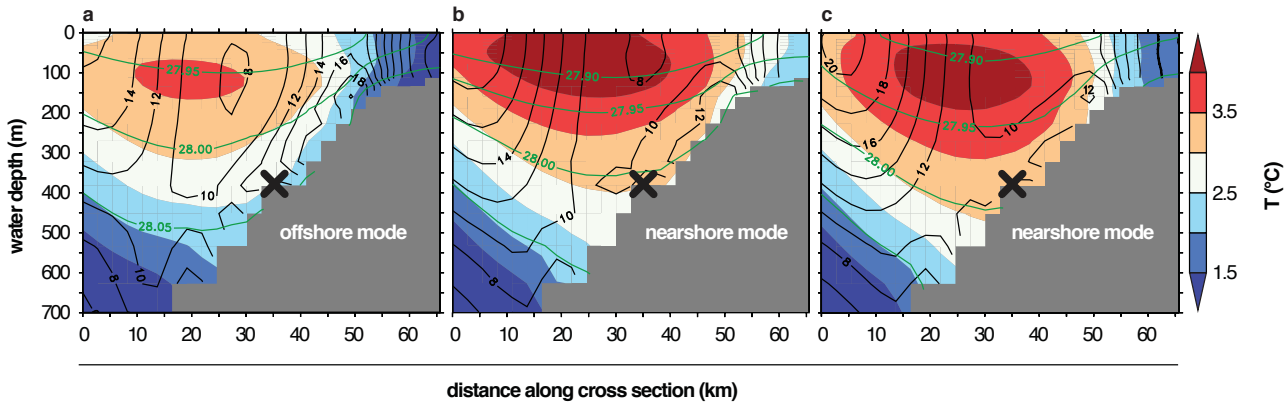
a
b
c
water depth (m)
offshore mode
nearshore mode
nearshore mode
distance along cross section (km)
T (°C)
3.5
2.5
1.5

Fig. 3

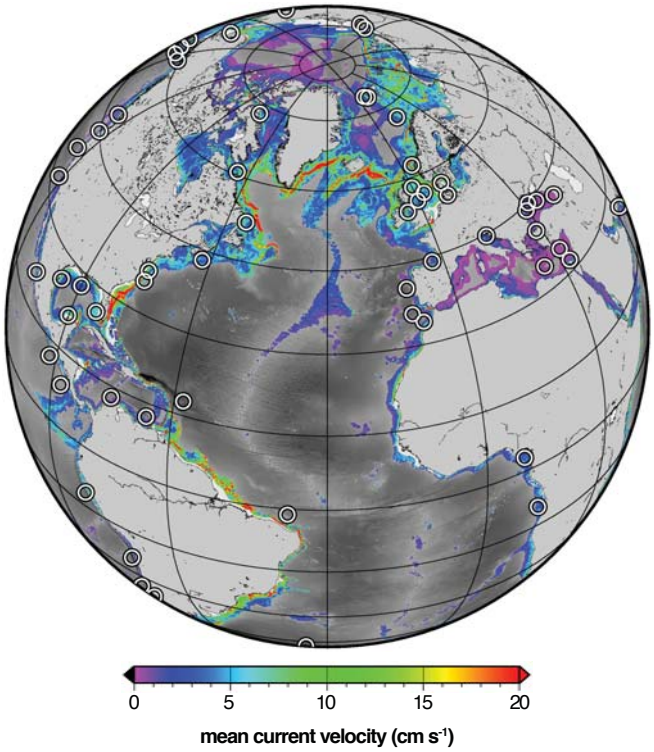

Tab.1

	sampling date (August 2012)	
	18/19	**30/31**
bottom water type	cAW	wAW
WSC mode	offshore	nearshore
max. MOx activity	3.2 nmol L^{-1} d^{-1}	2.1 nmol L^{-1} d^{-1}
CH_4 oxidised in seep area	17.82 kmol d^{-1} (0.28 t d^{-1})	5.57 kmol d^{-1} (0.09 t d^{-1})
max. MOB cells	29.7 × 10^3 mL^{-1}	3.65 × 10^3 mL^{-1}
max. MOB cells (% of tot. cells)	8.3	2.5
cell specific MOx activity	1.54 ± 0.34 × 10^{-2} fmol h^{-1} (0.22 – 5.74 × 10^{-2} fmol h^{-1})	1.66 ± 0.37 × 10^{-2} fmol h^{-1} (0.06 – 5.66 × 10^{-2} fmol h^{-1})